LAWRENCE
LIVERMORE
NATIONAL
LABORATORY

UCRL-JRNL-203338

A 3D Frictional Segment-to-Segment Contact Method for Large Deformations and Quadratic Elements

M.A. Puso, T.L. Laursen, J. Solberg

April 2, 2004

European Congress on Computational Methods in Applied Sciences and Engineering Proceedings

This work was performed under the auspices of the U.S. Department of Energy by the University of California, Lawrence Livermore National Laboratory under Contract No. W-7405-Eng-48.

European Congress on Computational Methods in Applied Sciences and Engineering
ECCOMAS 2004
P. Neittaanmäki, T. Rossi, K. Majava, and O. Pironneau (eds.)
R. Owen and M. Mikkola (assoc. eds.)
Jyväskylä, 24–28 July 2004

A 3D FRICTIONAL SEGMENT-TO-SEGMENT CONTACT METHOD FOR LARGE DEFORMATIONS AND QUADRATIC ELEMENTS

Michael A. Puso[⋆], Tod L. Laursen[†], and Jerome Solberg[⋆]

[⋆]Lawrence Livermore National Laboratory
The University of California
P.O. Box 808 Livermore, California 94550
e-mails: puso@llnl.gov, solberg2@llnl.gov

[†] Computational Mechanics Laboratory
Dept. of Civil and Environmental Engineering
Duke University,Durham N.C. 27708
e-mails: second.author@hut.fi

Key words: contact, quadratic elements, mortar, friction

Abstract. *Node-on-segment contact is the most common form of contact used today but has many deficiencies ranging from potential locking to non-smooth behavior with large sliding. Furthermore, node-on-segment approaches are not at all applicable to higher order discretizations (e.g. quadratic elements). In a previous work, [3, 4] we developed a segment-to-segment contact approach for eight node hexahedral elements based on the mortar method that was applicable to large deformation mechanics. The approach proved extremely robust since it eliminated the over-constraint that caused "locking" and provided smooth force variations in large sliding. Here, we extend this previous approach to treat frictional contact problems. In addition, the method is extended to 3D quadratic tetrahedrals and hexahedrals. The proposed approach is then applied to several challenging frictional contact problems that demonstrate its effectiveness.*

1 INTRODUCTION

Contact surfaces have been a very integral aspect of non-linear solid mechanics modeling for some time now. Nonetheless, it still remains one of the most challenging aspects of implicit structural mechanics and despite the research in the area, reliable and accurate algorithms are still not readily available. The most prominent algorithm for doing flexible body contact problems where there is large sliding is the node-on-segment contact algorithm developed by Hallquist [1]. This algorithm was developed for low order elements such as trilinear bricks and linear tetrahedrals and has numerous deficiencies such as locking, patch test failure and non-smooth behavior with large sliding that have been well documented in numerous papers [3, 4]. This standard version of node-on-segment is not applicable at all for quadratic elements since it performs so poorly in patch tests [2]

In this paper, the mortar method for large deformation solid mechanics presented in [3] and the frictional version in [4] is extended to treat quadratic elements. A standard application of the mortar method to quadratic elements would apply the slave side quadratic interpolation fields to interpolate the pressure fields. This is seen to work fine for mesh tying but, in the context of the mortar implementation given in [3], this will result in inconsistencies with the Kuhn Tucker conditions for the gap definitions. Of course one could modify the quadratic fields by using hierarchical versions but this may be unnecessary. Instead, it is seen that a linear interpolated stress fields are very effective and retain optimal convergence in spatial discretization error. In fact, by basing the linear interpolation fields on the corner nodes of the quadratic elements i.e. bilinear interpolation for twenty and twenty seven node hexahedrals and linear interpolation of the ten node tetrahedral, two pass contact can be applied such that no locking occurs.

An outline for this paper is as follows. In Section 1, a short description of the mortar implementation presented in [3, 4] is given. In addition, a short explanation of the extension to quadratic elements is provided. In section 2, a brief description of the numerical integration scheme is provided. Several numerical results are presented in Section 3.

2 Mortar Method Implementation

The classic mortar methods use the interpolation space of the non-mortar or slave side to interpolate the contact tractions. The n^1 nodes on the slave side define the interpolation from the displacement field shape functions denoted N_A^1 The opposing surface is defined as the mortar or master side composed of n^2 nodes and displacement shape functions denoted N_B^2 . Variations on this classical scheme are not unusual and are used here. The contact traction can be separated into normal $\boldsymbol{t}^N$ and frictional $\boldsymbol{t}^F$ parts where $\boldsymbol{\nu}$ is some surface normal such that

$$\begin{aligned} \boldsymbol{t} &= \boldsymbol{t}^N + \boldsymbol{t}^F \\ \boldsymbol{t}^N = p\,\boldsymbol{\nu} \qquad & \boldsymbol{t}^F \cdot \boldsymbol{\nu} = 0 \end{aligned} \tag{1}$$

The contact tractions are then interpolated

$$\boldsymbol{t}^N = \sum_{A=1}^{\tilde{n}^1} \tilde{N}_A^1(\boldsymbol{\xi}^1) p_A \boldsymbol{\nu}_A \qquad \boldsymbol{t}^F = \sum_{A=1}^{\tilde{n}^1} \tilde{N}_A^1(\boldsymbol{\xi}^1) \boldsymbol{t}_A \tag{2}$$

where p_A is a nodally defined pressure, $\boldsymbol{\nu}_A$ is a nodally averaged normal, $\boldsymbol{t}_A$ is the nodally defined frictional force where $\boldsymbol{t}_A \cdot \boldsymbol{\nu}_A = 0$, $\tilde{n}^1$ is the number of nodes on the slave side defining the pressure discretization and $\tilde{N}_A^1$ are the shape functions that define the type of discretization. In this work, three different interpolation schemes where exploited for the quadratic element implementation. The first just uses the slave side quadratic shape functions N_A^1 so that $\tilde{N}_A^1 = N_A^1$ and n^1 is just the number of nodes on the slave side. So for example, twenty seven node elements provide nine node patches with the usual two dimensional Lagrange shape functions defining the interpolation over the patch. The second scheme just uses the corner nodes of the quadratic patches. This would use a bilinear interpolation for the nine node and eight node patches and a linear patch for the six node patch seen in Figure 1. The third scheme interpolates the pressure piecewise over the nine, six and eight node patches. Referring to Figure 1, four bilinear patches define the pressure piecewise over the nine node patch, three linear patches are used to define the pressure over the six node patch and four linear and one bilinear patch are used over the eight node patch. For the second scheme, there about half as many contact constraints as there are nodes on the slave side. Consequently, it was found that a two pass application could be applied such that pressures where defined on both sides of the mesh and no locking occurs.

As presented in [3], the discrete normal contact gap g_A defined

$$g_A = \boldsymbol{\nu}_A \cdot \boldsymbol{g}_A \tag{3}$$

$$\boldsymbol{g}_A = \sum_B^{n^1} n_{AB}^1 \boldsymbol{x}_B^1 - \sum_C^{n^2} n_{AC}^2 \boldsymbol{x}_C^2 \tag{4}$$

and pressure p_A are the basis for the discrete form of the Kuhn Tucker conditions defined on the the non-mortar nodes A

$$g_A \le 0, \quad p_A \ge 0, \quad p_A g_A = 0 \quad \forall\, A = 1, \tilde{n}^1 \tag{5}$$

The contact weight values are given

$$n_{AB}^i = \int_\gamma N_A^1(\tilde{\boldsymbol{\xi}}^1) N_B^i(\tilde{\boldsymbol{\xi}}^i)\, d\gamma \tag{6}$$

A brief description of the process used to numerically integrate (6) is given in the next Section.

The contact slip increment is given [4]

$$\Delta \boldsymbol{s}_A = (\boldsymbol{I} - \boldsymbol{\nu}_A \otimes \boldsymbol{\nu}_A) \sum_{B,C}^{n^1,n^2} [(n^1_{AB}(t_{n+1}) - n^1_{AB}(t_n))\, \boldsymbol{x}^1_B(t_n) - (n^2_{AC}(t_{n+1}) - n^2_{AC}(t_n))\, \boldsymbol{x}^2_C(t_n)] \tag{7}$$

Using (7), the discrete Coloumb frictional Kuhn Tucker constraints are then given

$$\phi_A = \mu\, p_A - ||\boldsymbol{t}_A|| \geq 0, \quad \Delta \boldsymbol{s}_A = \zeta_A\, \boldsymbol{t}_A, \quad \zeta_A \geq 0, \quad \phi_A\, \zeta_A = 0 \quad \forall\, A = 1, \tilde{n}^1 \tag{8}$$

where μ is the Coulomb coefficient of friction. In this implementation, contact forces are evolved using a penalty regularization and a Uzawa version of the augmented Lagrange approach. Gap and slip distances can then be enforced to tight tolerances.

3 Numerical integration

The numerical integration of (6) is discussed in detail in [3]. It is also shown that care must be taken in the integration scheme such that momentum across the interface is conserved exactly. In the quadratic version of the integration scheme, the patches in Figure 1 are subdivided into bilinear and linear segments. These then become the segments over which integration of (6) is made. So for example, if the slave side was discretized using twenty node hexahedrals such that there were 100 eight node patches, the approach would subdivide the surface into 500 slave side (400 triangular and 100 quadrilateral) contact segments. The master side could be discretized using ten node tetrahedrals that would result in 300 master side segments. The algorithm given in [3] is then applied to integrate the contact segments. In short, for each slave segment k, a nearby candidate master segment l is found by rough search. The master segment l is then projected onto the slave segment k as shown pictorially in Figure 2. The intersected area is then discretized into triangles and (6) is integrated using Gauss-Radau integration rules.

4 Examples

4.1 Optimal Convergence

An internally pressurized thick sphere composed of twenty node hexahedrals is used to demonstrate optimal convergence for a 3D mesh with a curved *tied* dissimilar interface. The coarsest mesh is shown in Figure 3 and the effective stress is shown to vary smoothly. In Figure 4, the energy norm of the error is plotted for the thick sphere and demonstrates optimal convergence (slope = 2) for the different integration schemes: bilinear (scheme 2), two pass bilinear and a conforming mesh. Although not shown in Figure 4, scheme 1 and scheme 3 also produced similar errors to scheme 2 and converged optimally.

4.2 Large bending: locking free behavior

This example applies an external pressure uniformly over the exterior of a plane strain cantilever beam mesh such that a large pressure is experienced at the dissimilar contact interface. A bending moment is then applied to the beam such that it experiences large bending (Figure 5). The beam is composed of twenty seven node hexahedrals and friction is included at the interface. Our results (Figure 5) demonstrate that the two pass bilinear does not lock although there can be pressure modes that can exist on the interface. The final tip displacements for the one pass and two pass bilinear interpolation are within 0.5% of the conforming mesh result.

4.3 Large sliding: smooth results

This example demonstrates the superior response by mortar contact compared to node-on-segment contact in the event that nodes slide off contact surface boundaries. Two cubes are stacked vertically and are separated by a contact surface along a dissimilar interface. A vertical displacement is imposed on the top of the top block such that the blocks are uniformly compressed. The homogenous field is recovered exactly within machine precision since the formulation satisfies the patch test when the element segments are affine. The top of the top block is then displaced horizontally such that the top block first sticks due to friction and then eventually slips as seen in Figure 6. The left vertical face of the bottom block was fixed so that it would resist the frictional force. The results in Figure 6 were produced by a mesh composed of twenty seven node elements with two pass bilinear interpolated contact. Eight node elements were also used on a refined mesh such that twice as many elements were used per side (a factor of eight more overall). The vertical force versus horizontal displacement is shown plotted in Figure 7 for several cases:

1. two pass bilinear mortar contact applied (27 node hex mesh)
2. one pass bilinear mortar contact with lower surface as the slave (27 node hex mesh)
3. one pass bilinear mortar contact with upper surface as the slave (27 node hex mesh)
4. one pass bilinear mortar contact with lower surface as the slave (8 node hex mesh)
5. two pass node-on-segment contact (8 node hex mesh)
6. one pass node-on-segment contact with lower surface as the slave (8 node hex mesh)

From Figure 7 it is seen that results from cases 1,2 and 4 nearly overlap. Results from case 3 are just slightly softer. As expected, the node-on-segment results in cases 5 and 6 were not smooth , this is particularly true for the one pass case. Convergence was not attainable within fifty Newton iterations for several time steps with the two pass analysis yet the analysis was allowed to proceed. These hard points occurred at the spikes

in Figure 7. The one pass results blew up less than half way through the run and the analysis was halted.

5 Conclusion

A mortar frictional contact method [3, 4] was extended to treat quadratic elements. Several different pressure interpolations were considered. In fact a two pass bilinear interpolation scheme was proposed that doesn't encounter any locking although does posses pressure modes. These modes were not deleterious for the penalty regularized augmented Lagrange solution procedure but would need to be stabilized in the event that a direct Lagrange multiplier method was applied. The proposed method was shown to achieve full quadratic convergence in the energy of error for an internally pressurized sphere. Furthermore, the method was shown to be more robust than the node-on-segment approach in general.

REFERENCES

[1] J.O. Hallquist, G.L. Goudreau, and D.J. Benson. Sliding interfaces with contact-impact in large-scale lagrangian computations. *Computer Methods in Applied Mechanics and Engineering*, 51:107–137, 1985.

[2] P. Papadopoulos and R.L. Taylor. A mixed formulation for the finite element solution of contact problems. Technical Report UCB/SEMM Report 90/18, University of California at Berkeley, 1990.

[3] M.A. Puso and T.A. Laursen. A mortar segment-to-segment contact method for large deformation solid mechanics. *Computer Methods in Applied Mechanics and Engineering*, 59:315–336, 2004.

[4] M.A. Puso and T.A. Laursen. A mortar segment-to-segment contact method frictional contact method for large deformations. *Computer Methods in Applied Mechanics and Engineering*, 2004. to appear.

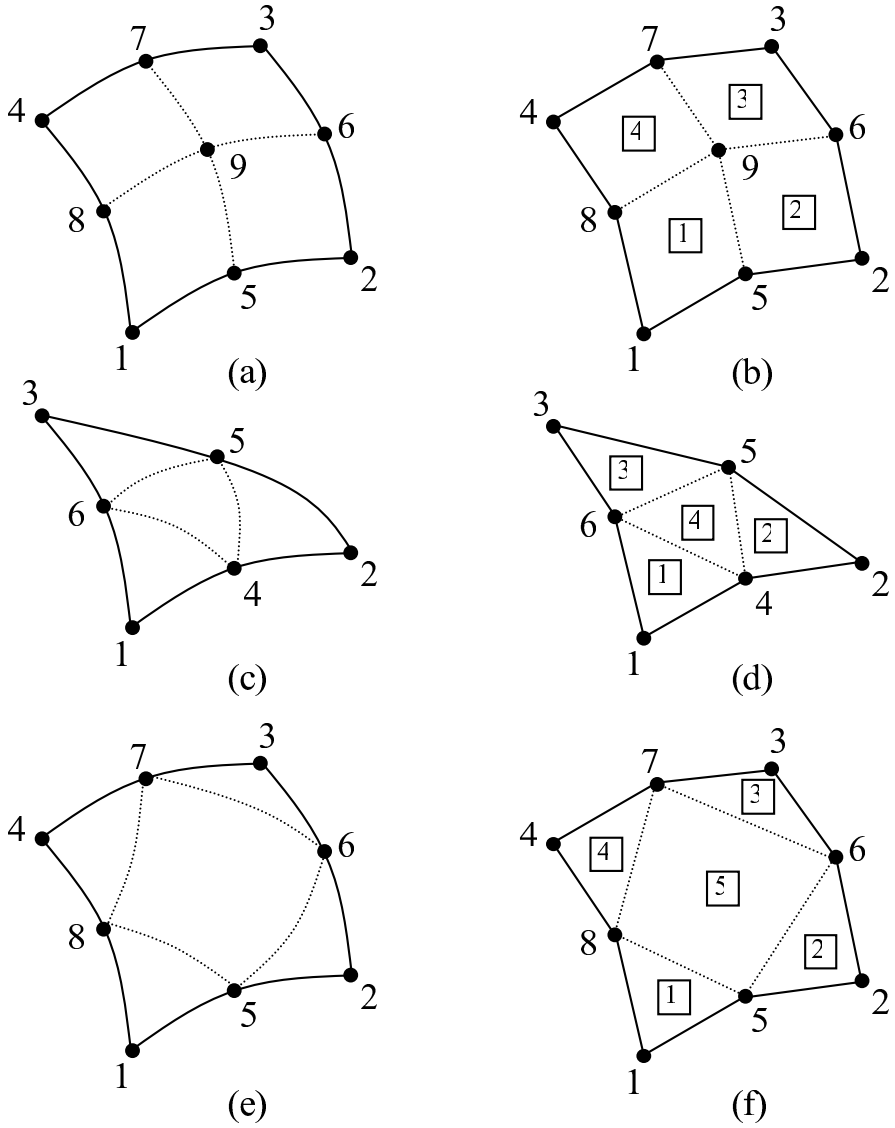

Figure 1: Division of quadratic patches into contact segments: (a) quadratic nine node patch (b) four quadrilateral segments (c) quadratic six node patch (d) three linear triangle segments (e) serendipity eight node patch (f) four linear triangle segments and one quadrilateral patch.

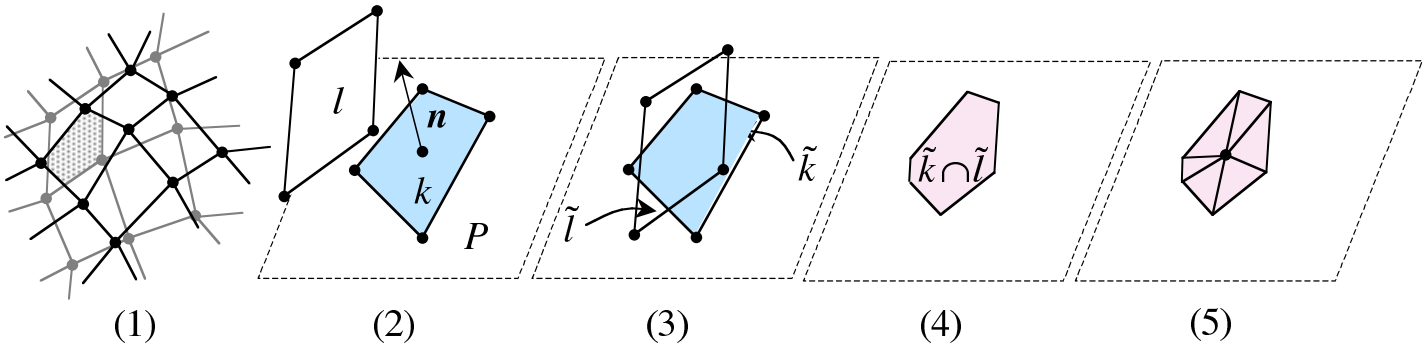

Figure 2: (a) Rough search identifying candidate master segment l for projection onto slave segment k. (b) Master segment l, slave segment k and plane $\boldsymbol{P}$ formed from the center point and normal $\boldsymbol{n}$ of k. (c) Facet $\tilde{k}$ and $\tilde{l}$ formed by projecting k and l onto plane. (c) Polygon formed from clipping algorithm. (d) Discretization of polygon into n_p triangular pallets.

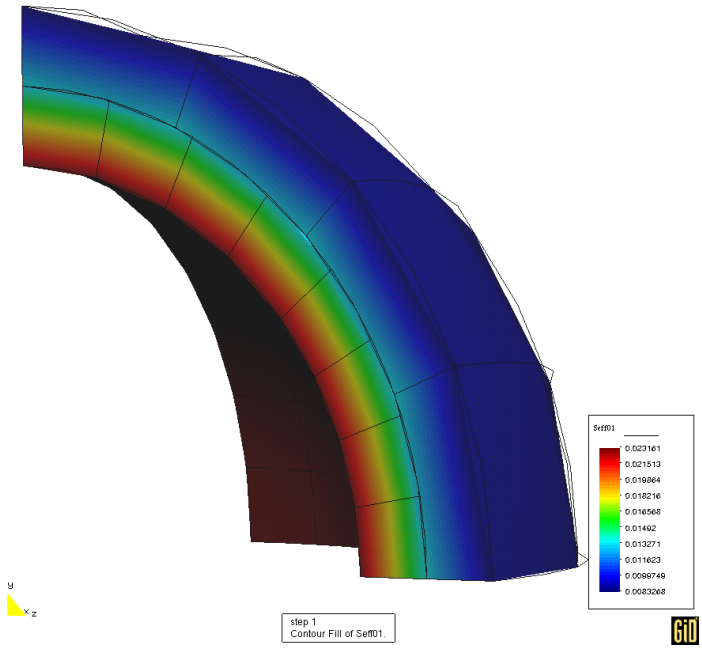

Figure 3: Effective stress plotted for coarsest pressurized sphere mesh where one pass bilinear mortar (scheme 2) was used. Mesh tying and not unilateral contact was used at the dissimilar interface.

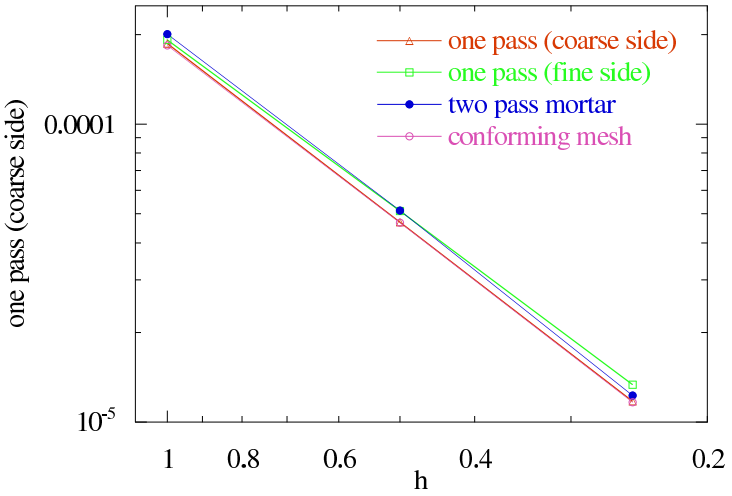

Figure 4: Plot of the energy norm of the error for internally pressurized sphere. Results are plotted for one pass bilinear mortar (scheme2) with coarse side and fine side as slave, two pass mortar and conforming mesh.

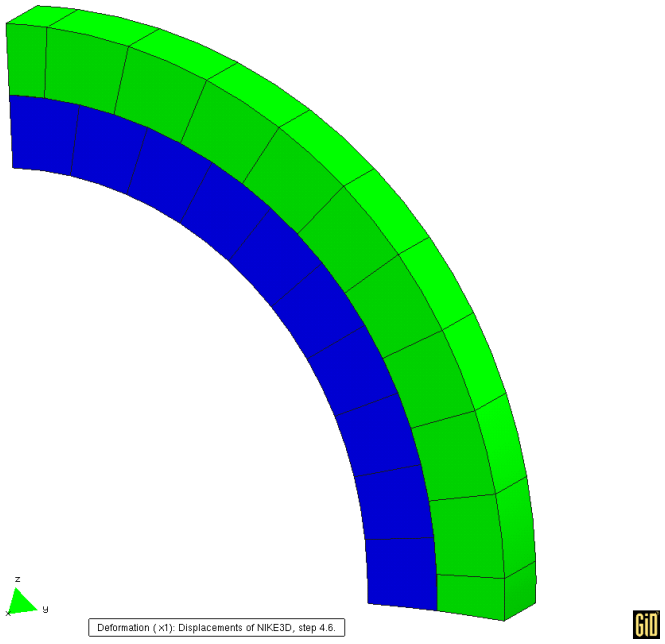

Figure 5: Bending example. Results shown from analysis using two pass bilinear interpolation.

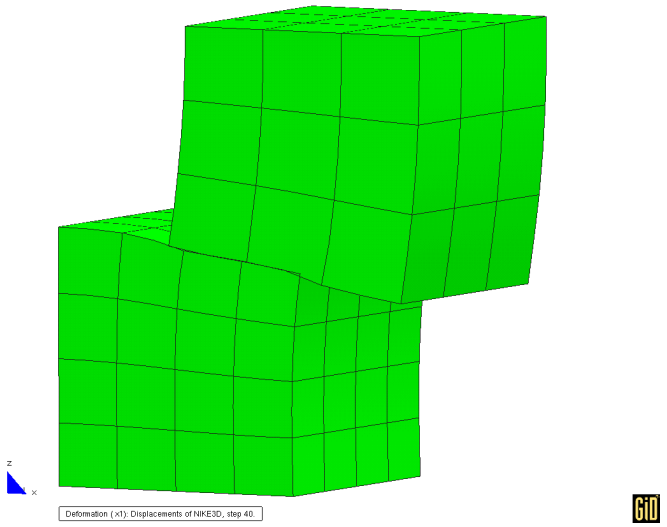

Figure 6: Blocks loaded compressively and then slide horizontally.

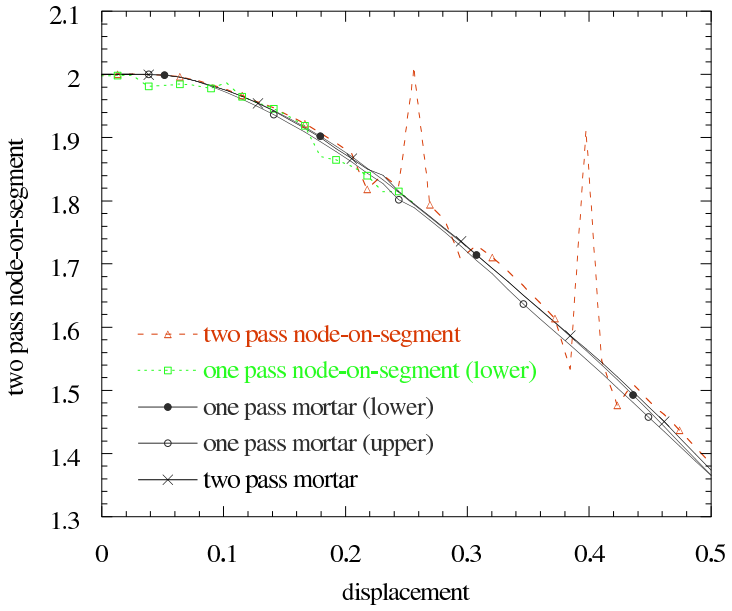

Figure 7: Vertical force versus horizontal displacement for sliding blocks example.